

Investigation of the magnetron balancing effect on the ionized flux fraction and deposition rate of sputtered titanium species for the high-power impulse magnetron sputtering pulses of different lengths

Cite as: J. Vac. Sci. Technol. A 41, 013003 (2023); doi: 10.1116/6.0002309

Submitted: 24 October 2022 · Accepted: 18 November 2022 ·

Published Online: 19 December 2022



Anna Kapran,^{1,2,3}  Vinicius G. Antunes,^{1,4}  Zdeněk Hubička,²  Charles Ballage,¹ and Tiberiu Minea^{1,a)} 

AFFILIATIONS

¹Laboratoire de Physique des Gaz et Plasmas—LPGP, UMR 8578, Université Paris Saclay, CNRS, 91405 Orsay CEDEX, France

²Institute of Physics v. v. i., Academy of Sciences of the Czech Republic, Na Slovance 2, 182 21 Prague 8, Czech Republic

³Faculty of Mathematics and Physics, Charles University, V Holesovickach 2, 180 00 Prague 8, Czech Republic

⁴Laboratoire des Technologies de la Microélectronique—LTM, UMR 5129 CNRS, Université Grenoble Alpes, CEA/LETI-Minatec, 38000 Grenoble, France

^{a)}Electronic mail: tiberiu.minea@universite-paris-saclay.fr

ABSTRACT

The study is focused on the impact of different magnetic field configurations of a high-power impulse magnetron sputtering (HiPIMS) in a nonreactive mode on the film precursors. Ionized flux fraction and total flux deposited onto the substrate were measured with the magnetic quartz crystal microbalance probe placed in front of the target racetrack. Particularly, we investigated the degree of magnetron balancing and the geometry of the magnetic field above the Ti target surface (4 in. diameter), as crucial factors influencing the thin film deposition, for different HiPIMS pulse lengths. Three unbalanced (II type) magnetron configurations have been chosen for this study: two symmetric geometries—with a regular magnetic field (B parallel to the target about 80 and 35 mT) and one asymmetric (highly unbalanced) magnetron configuration with an intermediate magnetic field (B parallel to the target about 48 mT). The HiPIMS was operated keeping constant the peak current at 43 A for C0-E0 and C10-E0 B-field configurations and a lower value, 33 A, when operating in C10-E10 configuration. In addition to the peak current, the pulse frequency was kept constant at 100 Hz but the pulse length (power on-time, T_{on}) was varied from 50 up to 100 μ s. Obviously, the pulse power and the average power continuously increase with the length of the pulse. The results reveal a significant difference in the trends of the deposition rate and ionized flux fraction reaching the substrate with respect to the degree of balancing of the magnetron. It was found that the ionized fraction of metal arriving at the substrate reaches its maximum for the pulse length between $T_{on} \approx 70$ – 80μ s in both symmetric cases, with strong and weak magnetic fields. The ionized fraction of Ti atoms in the asymmetric configuration increased in all measured range with the pulse length and the growth rate has a smooth increase.

Published under an exclusive license by the AVS. <https://doi.org/10.1116/6.0002309>

I. INTRODUCTION

Throughout the years, since Kouznetsov *et al.*¹ proposed high-power impulse magnetron sputtering (HiPIMS) as a new advanced sputtering technique, it remains one of the most in-demand technologies for thin film deposition. Compared to conventional dc magnetron sputtering (dcMS), HiPIMS plasma exhibits a highly

ionized flux fraction (IFF) of sputtered material contributing to the film growth. It is due to the more efficient sputtering of the target operated at higher voltages in HiPIMS compared to the dcMS case, the higher ionization induced by the much higher operation current (typically two orders of magnitude), as well as of the effectiveness of the magnetic trap created in front of the target by a

magnet pack placed behind the target.^{2–6} The magnetic field (**B**-field) produced by the magnets assembly traps only the electrons, which under the high electric field applied during the HiPIMS pulse, enhances the plasma density ($>10^{19} \text{ m}^{-3}$) near the target, the so-called ionization region (IR). The strong effect of the magnetron assembly configuration on the HiPIMS discharge characteristics has been observed in various experiments.^{7–12} By all these contributions, it was proved that **B**-field strength and the magnetic field configuration play one of the major roles in a proper design of the sputtering process. However, the effect of the cathode **B**-field on the deposition process in HiPIMS is not fully investigated and still remains unclear in some aspects regarding ion transport in HiPIMS plasma beyond the IR.

As reported before,^{8,9,13–15} a change of the magnet pack design makes it possible to improve the ion bombardment on the substrate by deriving more ions from the IR towards the diffusion region. Alami *et al.*⁸ investigated four magnetron assembly designs (balanced/unbalanced with strong/weak magnetic fields) for their impact on HiPIMS discharge operating in metallic and reactive modes. It has been observed that important phenomena occurring in HiPIMS plasma, such as gas rarefaction in the region close to the target, a side-wall loss of the metal ions, and other transport processes, are strongly depended on and can be effectively controlled by the variations of balancing degree. Subsequently, these findings have been confirmed by Hajihoseini *et al.*⁹ Their study clearly revealed a high sensitivity of HiPIMS discharges characteristics to the variations in the degree of balancing of the magnetron. The more strongly the magnetron is unbalanced (type II configuration), the higher the ionization flux fraction is. In contrast to the balanced type, an unbalanced magnets assembly produces the **B**-field spreading far beyond the IR; thus, the plasma ions can more efficiently assist the film growth.¹⁶

One suggested way to improve the deposition rate of sputtered material is to apply **B**-field of reduced strength in the region close to the cathode surface. Ehasarian,¹⁷ pursuing this approach, obtained a niobium deposition rate representing 90% of the deposition rate in dcMS sputtering. This was made possible through the lowering of the radial component of **B**-field strength above the cathode surface of less than 40 mT. Mishra *et al.*¹⁸ found that the deposition rate of titanium increases by up to a factor of six at the substrate position (10 mm away from the target) if the magnetic field in the IR is lowered by 30%. These results have been later confirmed by Čapek *et al.*¹⁹ when studying the niobium-deposited flux. The growth of deposition rate with decreasing **B**-field in the IR is a result of reducing the presheath potential barrier, i.e., the voltage drop over the IR. An immediate consequence of this voltage drop is the back-attracted to the target of the metal atoms ionized in the IR, one of the major drawbacks of the HiPIMS. The back-attraction effect drastically influences the deposition rate in HiPIMS.^{7,20,21} As the magnetic field strength decreases, the sheath in front of the target is also affected, becoming wider. The lowered electrical field across the sheath helps a large fraction of ionized sputtered particles to escape from the magnetic trap, i.e., the ionization region.

An extensive set of experiments has been performed by Hajihoseini *et al.*^{9,22} to study the effect of the magnetron **B**-field on a nonreactive HiPIMS discharge with a titanium target. For

HiPIMS operated at constant peak current and constant average discharge power, it was found that a decrease in the magnetic field strength brings an enhanced deposition rate (increased by 38%).¹⁸ The ionization fraction, measured at the distance from the target where the substrate is typically placed ($z = 70 \text{ mm}$), was found to be increased by 53%. Operating the HiPIMS discharge in the fixed current mode, ionization probability α increased with increasing the magnetron **B**-field.²³ In this case, the probability of back-attraction remained roughly constant.

Shortening the pulse length is another well-known way to diminish the probability of the ions returns to the near-target region. It was demonstrated previously in Refs. 24–28 that when operating HiPIMS with shortened pulses, the self-sputtering mode is reduced since the metallic species do not spend enough time in the high-density plasma region to be ionized there. Shimizu *et al.*²⁸ investigated a contribution of ion fluxes coming during the afterglow. By shortening the HiPIMS pulse length, it was found that the contribution to the outward flux of film-forming species from the afterglow increases significantly. HiPIMS discharges at a constant peak current density of about 1.10 A/cm^2 showed a 45% increase in the deposition rate, by shortening the pulse duration from 200 to $50 \mu\text{s}$. Shorter pulse lengths do not allow a significant amount of gas rarefaction or self-sputtering to develop. Significant gas rarefaction can occur for longer HiPIMS pulses ($T_{\text{on}} > 50 \mu\text{s}$).²⁹ It was demonstrated by Konstantinidis *et al.*³⁰ that the deposition rate increased by 20%–70% compared with the dcMS values as the pulse length shortened from 20 to $5 \mu\text{s}$ for the identical average power. However, there is no mention on the fraction of ionized precursors contributing to the film.

In the present study, inspired by the experimental approach found in Ref. 9, we investigate the IFF and deposition rate of sputtered titanium at the substrate position by varying the magnetron **B**-field strength, degree of balancing, and pulse length on HiPIMS sputtering processes. The pulsing frequency was kept constant, as well as the peak current, aiming to keep (almost) constant the sputtering conditions on the target. However, in the present study, the length of the pulse was gradually shortened, and, consequently, the pulse power and average power transferred to the discharge decreased, which directly impacts the probability to ionize the sputtered atoms.

II. EXPERIMENT

The experiments were performed in DIVA (Dispositif d'ionisation de la Vapeur Atomique, Orsay, France) magnetron sputtering system, which is schematically represented in Fig. 1, the same used in Ref. 9.

The sputtering system consists of a cylindrical vacuum chamber made from stainless steel with a diameter of 45 cm and height of 50 cm, which reaches a base pressure below $5 \times 10^{-5} \text{ mbar}$ with a turbomolecular pump (Pfeifer Vacuum, HiPace 700, Germany) combined with a dry vacuum pump (Pfeiffer, ACP15). The pressure is monitored with the vacuum gauges (Pfeifer Vacuum PKR 251, Germany and MKS 627 BX). A throttle valve (MKS 623B, USA) installed between the vacuum chamber and the turbo-pump is used to adjust and keep constant 1 Pa of the working gas, Ar of high purity 99.9999% (Alphagaz 2, USA).

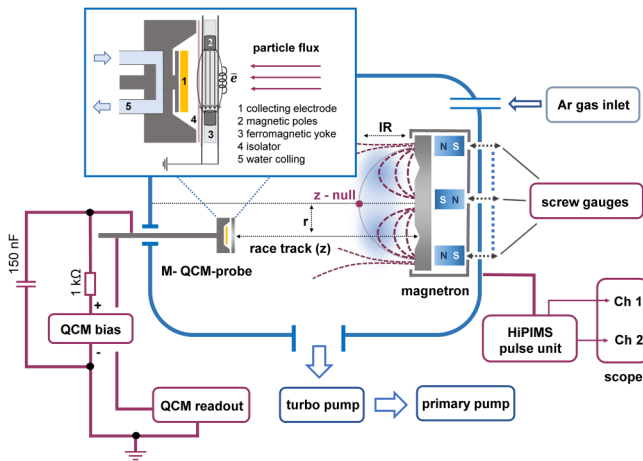


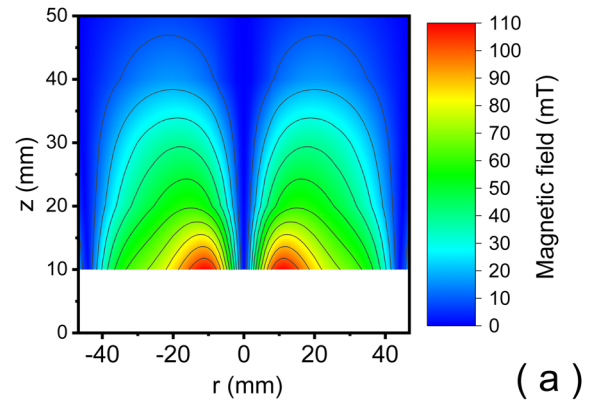
FIG. 1. Experimental setup. The inset shows the detail of the magnetic quartz crystal microbalance (M-QCM).

The inlet flow rate was 50 sccm. HiPIMS discharge was supplied with a HiPSTER 1 (Ionautics, Sweden) pulse power supply with a DC source (Technix SR1.5-N-1500, France). The pulse current and voltage on the target were monitored and recorded in real-time using a digital oscilloscope (LeCroy 625zi, USA).

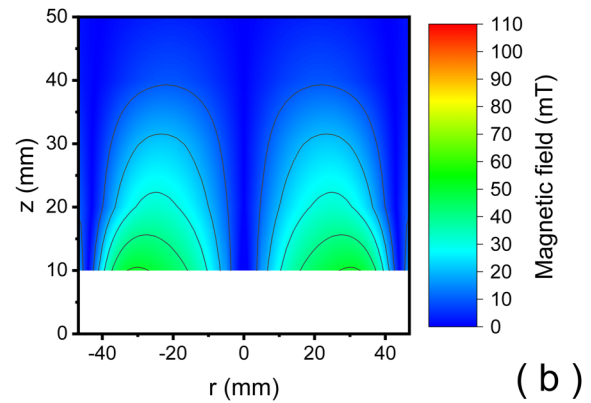
For all measurements, the pulsing frequency of 100 Hz was kept constant. For that reason, as the length of the pulse was gradually shortened the pulse power and average power absorbed in the discharge decreased, which is directly related to the probability to ionize the sputtered atoms.

The magnetron assembly consisted of a central (C) and edge (E) moveable magnet pack and a circular 4-in. titanium target (V-Tech, Genoa, UK). The magnet pack has two-micrometer screws that independently control the displacement of C and E. Thanks to this design, the degree of balancing can be easily varied, without breaking the vacuum. In this study, we investigated three degrees of balancing: two symmetric (weakly unbalanced), where C and E are equidistant to the back of the target at 0 (strong \mathbf{B} -field, denoted C0-E0) and 10 mm (weak \mathbf{B} -field, denotes C10-E10), and one asymmetric (strongly unbalanced), where C is at 10 and E at 0 mm (reduced \mathbf{B} -field, denoted C10-E0). Figure 2 shows the maps associated with each one of these magnets configurations. The parallel component of the magnetic field has been measured above 11 mm from the target until 50 mm using Lake Shore 425 Gauss meter.

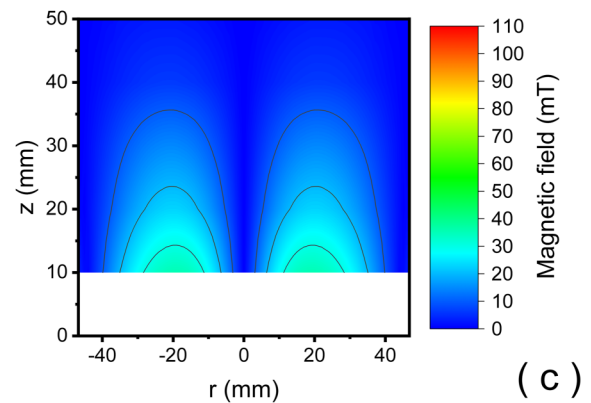
For the quantitative determination of ionized flux fraction, a modified magnetized QCM probe (M-QCM) with heating control has been used. The probe was first introduced by Hubička *et al.* as a modification of the gridded ion flux analyzer.^{31,32} The M-QCM-sensor is placed 60 mm away from the target facing the racetrack. It contains three main parts, which are the gold-coated collecting electrode, magnetic trap, and deposition rate measuring unit. A schematic representation of the device can be seen in the inset of Fig. 1. The commercially available quartz crystals (Inficon, USA) with a native frequency of 6 MHz are mounted into



C (0mm) E (0mm), $|\mathbf{B}_{||}| = 80$ mT



C (10mm) E (0mm), $|\mathbf{B}_{||}| = 48$ mT



C (10mm) E (10mm), $|\mathbf{B}_{||}| = 35$ mT

FIG. 2. 2D (r, z) magnetic field distribution above the magnetron target. Color scale indicates the intensity of the parallel component of \mathbf{B} -field. Each configuration refers to the displaced distance of each magnet from the target backing plate: (a) C0-E0; (b) C10-E0; and (c) C10-E10.

24 September 2023 09:15:23

a water-cooled holder. Continuous cooling minimizes the signal instabilities caused by crystal heating. The M-QCM probe was connected to a thickness monitor (STM-2, Inficon, USA).

The magnetic trap configuration of the sensor allows us to enhance the accuracy of the measurement by separating electrons from the total deposited flux onto a crystal. The magnetic trap placed in front of the probe orifice consists of a ferromagnetic yoke and cylindrical SmCo magnets of 8 mm diameter and 5 mm length. The small size of the magnet poles eliminates an additional ionization close to the crystal surface, which can be caused by electron trapping. Magnetic trap produces a stationary magnetic field of 0.4 T parallel to the crystal surface, which is not sufficient to disturb the magnetron magnetic field. However, a major part of incoming electrons is caught by these magnetic field lines due to their small gyro-radii, while ions can cross the lines and reach the QCM-sensor.

The sensor can be either grounded for measuring the total flux deposited on a crystal surface or positively biased for collecting the neutral flux only. The bias voltage was applied to a crystal through a 1 kΩ resistor to prevent the formation of the arc on the electrode surface. A 150 nF capacitor inserted in parallel into the circuit blocks the DC current to the electrode. For details, the interested reader can see Refs. 31 and 32.

M-QCM probe has an essential advantage in operation compared with the frequently used gridded ion flux analyzers. There are several studies^{33–35} that indicated the necessity and the complexity of a calibration procedure for the instrument, caused by the throughput and the geometry of the grid system. Since the grids are substituted by magnets in front of the sensor, M-QCM provides a significantly higher signal with no calibration required prior to the measurements.

All data were acquired and recorded within 1 min with a time step of 0.1 s. The interval between the measurements rolled for 2 min after the proper stabilization of the system which took tens of seconds. To minimize the noise effect on the recorded signal, the deposition rate of neutrals ($\Gamma_{neutral}$) or total (Γ_{total}) atoms was assessed as the slope of a linear fit on a growing film thickness obtained from the QCM readout. A positive bias of +37 V was applied on the collecting electrode to determine the contribution of neutral flux, repelling the metal ions from the probe. The total flux was obtained without bias. Thus, the contribution of the metal ions can be easily assessed using the formula:

$$(\Gamma_{ions}) = \frac{\Gamma_{total} - \Gamma_{neutral}}{\Gamma_{total}}. \quad (1)$$

The error in deposition rates is estimated to be within 15% for a single measurement.

III. RESULTS AND DISCUSSION

The typical series of current and voltage waveforms of the HiPIMS discharge recorded for different strengths of **B**-field are presented in Fig. 3. The pulse length was varied from 50 up to 100 μs, with the peak current kept constant at 43 A for C0-E0 and C10-E0 **B**-field configurations and slightly lower, at 33 A, when operating in C10-E10 configuration. The pulse cathode voltage was

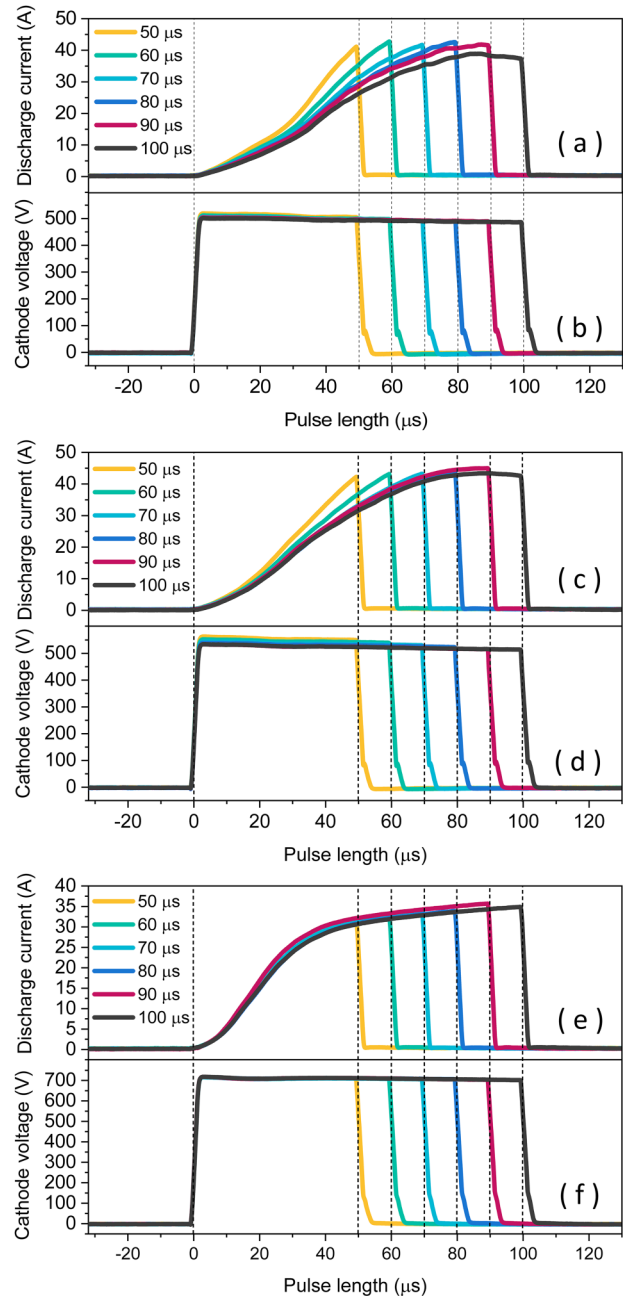


FIG. 3. HiPIMS current (top panel) and voltage (bottom panel) waveforms recorded for different balancing degrees of the magnetic field. The current and voltage peaks correspond to the magnet configurations: (a) and (b) C0-E0, (c) and (d) C10-E0, and (e) and (f) C10-E10.

similar about $U_c \approx 500$ V for both slightly unbalanced C0-E0 and C10-E0 cases, while for C10-E10, it was increased at $U_c \approx 700$ V. In spite of the voltage increase, the maximum pulse current decreased, expected behavior for the weaker electron trapping (C10-E10). In

24 September 2023 09:15:23

this case, the magnetic field magnitude parallel to the target surface is lower (see Fig. 2) resulting in less intensive ionization of magnetron plasma and smaller discharge currents.

The degree of balancing influences both the cathode voltage and discharge current,^{9,10,28} as shown in Fig. 3. For example, the C10-E10 peak current increases sharply while C0-E0 increases smoothly, following the decrease of **B**-field strength. Besides, the C0-E0 current has been split among T_{on} pulses more than C10-E0, and C10-E10 has almost a perfect match over all curves.

Figure 3 also reveals variations of the discharge current rise-time, especially for longer pulses (80–100 μ s). This behavior can be caused by the gas rarefaction effect. The first considered magnetic configuration C0-E0 with the strong magnetic field above the target surface exhibits the current slowly decreasing after 85 μ s of the pulse [Figs. 2(a) and 3(a)]. That is mainly due to the sputtered titanium particles expelling the buffer gas from the region near the target but also to the important ionization of the argon gas²⁹ and the gas recycling³⁶ resulting in lower ion density at that region, thereby preventing the further rise of the discharge current.

To preserve the same peak pulse current, by switching the magnetron to C10-E0 mode [highly unbalanced, Figs. 2(b) and 3(b)] and decreasing the parallel magnetic field strength, the cathode voltage has to be increased to 50 V. However, the typical growth of the discharge current demonstrates the similar character of the discharge in this case compared to the magnetron with the strongest **B**-field (C0-E0).

Further, a serious increase of the voltage applied to the target, up to 700 V (40% higher compared to the case of the strongest parallel magnetic field), is required for the weakest magnetron field C10-E10 [Fig. 2(c)] to reach comparable, but lower currents (10% lower peak current). In addition, there is no sign of the current decrease by the end of the pulse [Fig. 3(c)]. Consistent with the previous conditions, this could mean less gas rarefaction in the IR. On the one hand, a lower sputtering wind from the target (since the current is lower) of Ti atoms pushes less argon out of the IR, and also less argon is ionized. On the other hand, the higher applied voltage involves a strengthened back-attraction effect in the target-near region. Sputtered Ti^+ incoming to the target compensates the loss of argon ion contribution to the discharge current, which slightly and smoothly grows until the end of the pulse.

The average discharge power was calculated from the waveforms of discharge current and cathode voltage (Fig. 3) by the following equation:

$$P_{avg} = \frac{1}{T_p} \int_0^{T_p} U_c(t) I_d(t) dt, \quad (2)$$

where T_p is the pulse period, and U_c and I_d are the cathode voltage and the discharge current, respectively. The pulse power values were obtained from the formula according to the pulse length variation,

$$P_{pulse} = \frac{1}{T_{ON}} \int_0^{T_{ON}} U_c(t) I_d(t) dt, \quad (3)$$

where T_{on} is the length of “on” time in the HiPIMS pulsing cycle (pulse length).

The average power calculated according to Eq. (2) and the pulse power calculated according to Eq. (3) are not constant in this work and they increase with the pulse length as shown in Fig. 4. This is a significant difference with respect to the previous works.^{9,22}

Figure 4 illustrates the titanium IFF and deposition rate onto the probe surface versus the pulse length, from 50 μ s up to 100 μ s, with the corresponding evolutions of the average discharge power and pulse power. As the graphs show, the IFF and deposition rate exhibit similar behavior for both (strong and weak) symmetric magnetron configurations.

For a strong magnetron magnetic field (C0-E0), the measured titanium IFF demonstrates an increasing trend with the prolongation of the pulse duration up to 80 μ s with the peak of 14% of metal ions incoming to the substrate. This maximum is about 12% at 70 μ s when the magnetic trap is less effective, operating the discharge with the weakest magnetic configuration (C10-E10). After reaching their peaks, the IFF drops down sharply, despite of the increase of the pulse power with the pulse duration [Figs. 4(e) and 4(f)]. With the pulse length of 100 μ s, the IFF falls to 10% (C0-E0) and 8% (C10-E10), which is well consistent with the data obtained previously in Ref. 9. The IFF of 11% has been reported for the magnetic field C0-E0 with the peak current density of 0.5 A/cm² and the pulse frequency of 143 Hz (no data for C10-E10 were published).

Several phenomena can lead to such (unexpected) behavior. This drop in the ionized flux can be a consequence of the sputter wind effect (gas rarefaction) occurring near the target in the case of field C0-E0. Indeed, the lower the pressure in the IR, the higher the fraction of neutrals crossing the IR without collisions (ballistic transport of Ti^+),³⁷ and, hence, increasing the flux of neutrals to the substrate decreases the ionized flux fraction. Another explanation could be the increase of the back-attraction of the ions with the pulse length,²⁵ which also decreases the IFF. Another possibility could also be a modification of the angular distribution of the fraction of ions leaving the IR on the side with respect to the fraction propagating forward. Hence, this can reduce also the IFF.³⁸ One or several of these phenomena can act simultaneously affecting the IFF for pulses beyond 80 μ s.

Turning back to the current waveforms of C0-E0 discharge [Fig. 3(a)], one can notice that the discharge current continuously rises during the pulse, as well as the power, up to 80 μ s where we observe the highest ionization degree of sputtered species reaching the probe surface. Within the interval from 50 to 80 μ s of the pulse, no significant “sputter wind effect” (including rarefaction) occurs. However, extending the pulse length further leads to the formation of the so-called plateau phase of the current, which indicates the sputter wind in our case of nonreactive sputtering. By increasing the pulse length from 50 to 100 μ s, the deposition rate increases linearly in both cases of symmetric magnetron configurations [Figs. 4(a) and 4(e)]. One can see a similar decrease of IFF of Ti after 70 μ s for magnetic field C10-E10, even if the current plateau is never reached. But we stated above that due to higher cathode voltage $U_c \approx 700$ V the back-attraction of sputtered Ti^+ increases. This can be the reason for higher loss of Ti^+ for longer pulses and consequently the lower signal of Ti^+ on the QCM electrode.

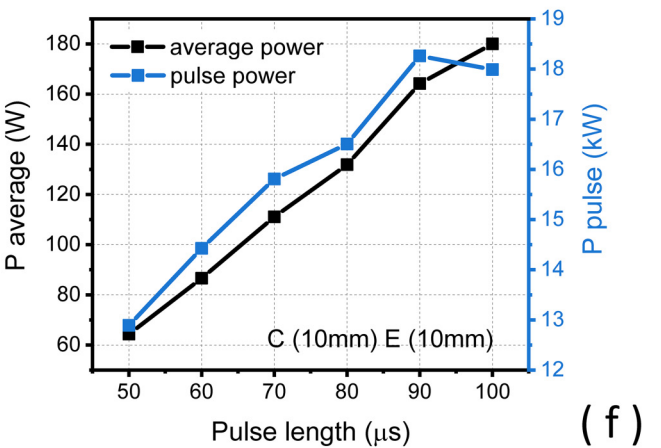
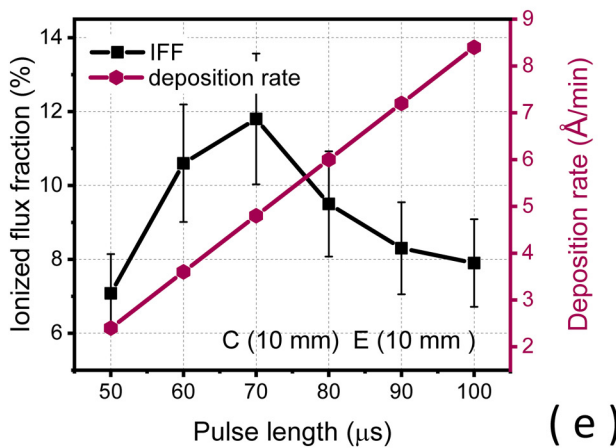
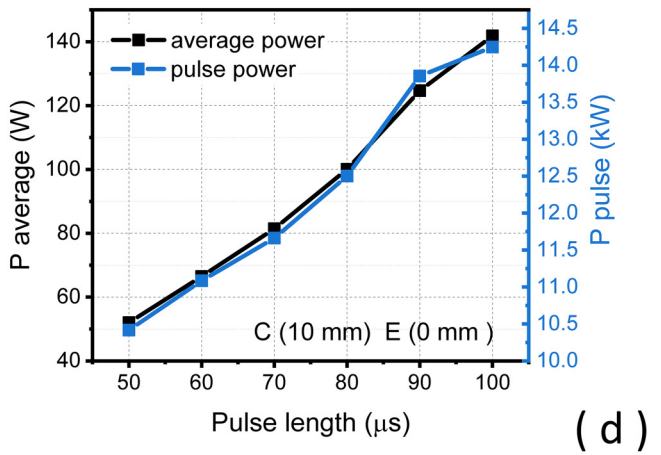
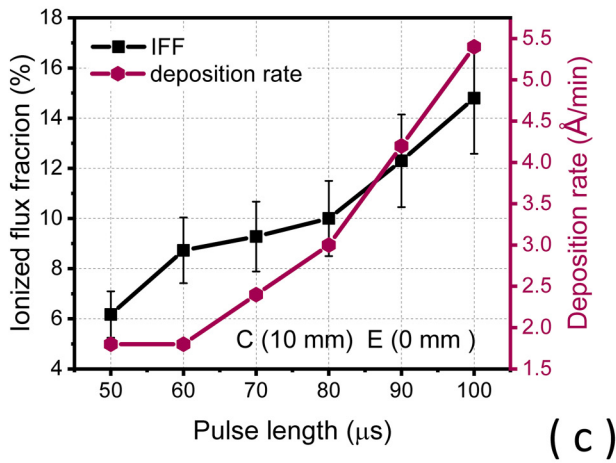
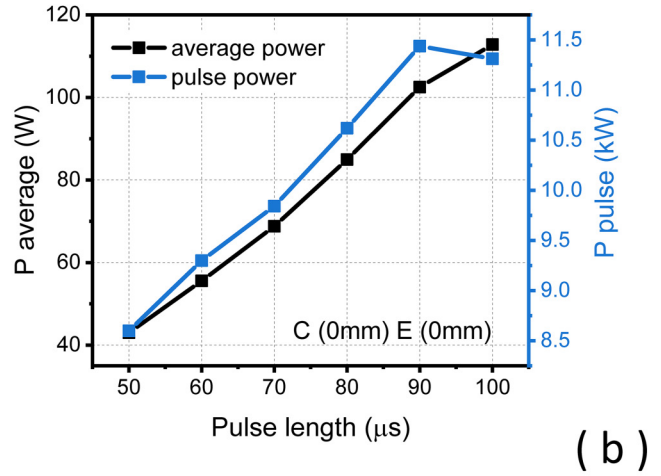
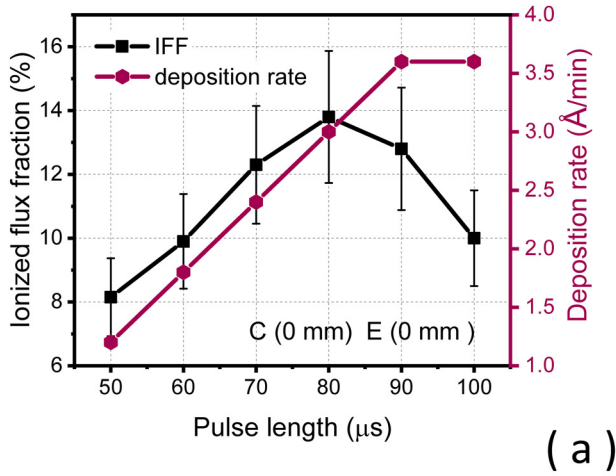


FIG. 4. Ionized flux fraction (left column, left y axis) and deposition rate (left column—right y axis) of Ti in correspondence with the average power (right column—left y axis) and pulse discharge power (right column—right y axis) investigated for various HiPIMS pulse lengths at a constant frequency of 100 Hz. The graphs correspond to the magnet configurations: (a) and (b) C0-E0, (c) and (d) C10-E0, and (e) and (f) C10-E10.

24 September 2023 09:15:23

In the case of the magnetic field C10-E0, the IFF exhibits a different trend [Fig. 4(c)]. The ionized flux fraction toward the collecting M-QCM surface continuously increases when the pulse length increases. The faster increase of IFF for pulses with a length of 50–70 μs is connected with a parabolic dependence of the deposition rate growth. It could mean that Ti^+ losses due to back-attraction to the target are lowered in this case. An enhanced amount of ionized species reaching the probe might be the result of back-attraction reduced due to tuning the magnetron into an asymmetric geometry (highly unbalanced). In the C10-E0 mode, the magnetic field lines extend toward the substrate, and electrons gyrating around these lines can carry the ions away from the target region by ambipolar diffusion.

IV. CONCLUSIONS

The HiPIMS magnetron with titanium target was studied for different magnetic field configurations. It used the symmetric magnetron configurations with a strong magnetic field (C0-E0) and weak magnetic field (C10-E10). Furthermore, the asymmetric magnetron (C10-E0) was used as well. The ionized flux fraction of sputtered titanium and deposition rate were measured for different pulse lengths and magnetic field configurations. The pulse power and the average power continuously increase with the length of the pulse. It was found that IFF has a maximum value for the pulse length between ≈ 70 and $80 \mu\text{s}$ in the case of strong and weak fields (C0-E0) and (C10-E10), respectively, slightly unbalanced. The IFF of Ti atoms in the highly unbalanced magnetic field configuration (C10-E0) increased in all measured ranges of pulse lengths and the growth rate slightly increased. Based on the study of Rudolf *et al.*,¹⁰ we argue that this unbalanced configuration is responsible for reduced Ti^+ back-attraction and ionization degree of Ti atoms increase in the place of the probe. The growth rate parabolic increase can be justified for the same reason.

These results suggest that there is an optimum of the applied pulse power (or pulse length) to reach the maximum IFF of sputtered species onto the substrate. Beyond this maximum, and for longer pulses, the deposition rate increases due to mainly neutral particles and the ion assistance effect weakens. Also, for the asymmetric configuration (C10-E0), both the IFF and the deposition rate increase with the pulse power, but for the same pulse length, both of these are lower compared to the symmetric case (C0-E0).

ACKNOWLEDGMENTS

The authors gratefully acknowledge Ovidiu Vasilovici (LPGP, Université Paris Saclay) for technical assistance. The work was partly supported by the Czech Science Foundation (Project No. 21-04477S) and the Operational Programme Research, Development and Education (Project No. SOLID21-CZ.02.1.01/0.0/0.0/16_019/0000760) financed by the European Structural and Investment Funds and the Czech Ministry of Education, Youth and Sports.

AUTHOR DECLARATIONS

Conflict of Interest

The authors have no conflicts to disclose.

Author Contributions

Anna Kapran: Data curation (lead); Formal analysis (lead); Investigation (equal); Methodology (equal); Validation (equal); Visualization (lead); Writing – original draft (lead); Writing – review & editing (equal). **Vinicius G. Antunes:** Investigation (equal); Methodology (equal); Validation (equal); Writing – review & editing (equal). **Zdeněk Hubička:** Funding acquisition (equal); Investigation (supporting); Validation (equal); Resources (equal); Writing – review & editing (equal). **Charles Ballage:** Investigation (supporting); Resources (equal); Writing – review & editing (supporting). **Tiberiu Minea:** Conceptualization (lead); Funding acquisition (equal); Investigation (equal); Methodology (equal); Project administration (lead); Resources (lead); Supervision (lead); Validation (equal); Writing – review & editing (equal).

DATA AVAILABILITY

The data that support the findings of this study are available from the corresponding author upon reasonable request.

REFERENCES

- V. Kouznetsov, K. Macák, M. Shneider, U. Helmersson, and I. Petrov, *Surf. Coat. Technol.* **122**, 290 (1999).
- U. Helmersson, M. Latteman, J. Bohlmark, A. P. Ehasarian, and J.-T. Gudmundsson, *Thin Solid Films* **513**, 1 (2006).
- M. Samuelson, D. Lundin, J. Jensen, M. A. Raadu, J.-T. Gudmundsson, and U. Helmersson, *Surf. Coat. Technol.* **205**, 591 (2010).
- J.-T. Gudmundsson, N. Brenning, D. Lundin, and U. Helmersson, *J. Vac. Sci. Technol. A* **30**, 030801 (2012).
- J.-T. Gudmundsson, *Plasma Sources Sci. Technol.* **29**, 113001 (2020).
- J. Bohlmark, U. Helmersson, M. Van Zeeland, I. Axnäs, J. Alami, and N. Brenning, *Plasma Sources Sci. Technol.* **13**, 654 (2004).
- J. W. Bradley, A. Mishra, and P. J. Kelly, *J. Phys. D: Appl. Phys.* **48**, 215202 (2015).
- J. Alami, V. Straňák, A.-P. Herrendorf, Z. Hubička, and R. Hippler, *Plasma Sources Sci. Technol.* **24**, 045016 (2015).
- H. Hajihoseini, M. Čada, Z. Hubička, S. Ünalı, M. A. Raadu, N. Brenning, J. T. Gudmundsson, and D. Lundin, *Plasma* **2**, 201 (2019).
- M. Rudolf, N. Brenning, H. Hajihoseini, M. A. Raadu, T. M. Minea, A. Anders, J.-T. Gudmundsson, and D. Lundin, *J. Phys. D: Appl. Phys.* **55**, 015202 (2022).
- J. Lin and X. Zhang, *Surf. Coat. Technol.* **438**, 128417 (2022).
- H. Yu, L. Meng, M. M. Szott, J. T. McLain, T. S. Cho, and D. N. Ruzic, *Plasma Sources Sci. Technol.* **22**, 045012 (2013).
- B. Window and N. Savvides, *J. Vac. Sci. Technol. A* **4**, 453 (1986).
- N. Savvides and B. Window, *J. Vac. Sci. Technol. A* **4**, 504 (1986).
- S. E. Rodil and J. J. Olaya, *J. Phys.: Condens. Matter* **18**, S1703 (2006).
- A. Anders, *J. Vac. Sci. Technol. A* **28**, 783 (2010).
- A. Ehasarian, UK Patent No. GB2437730 (2006).
- A. Mishra, P. J. Kelly, and J. W. Bradley, *Plasma Sources Sci. Technol.* **19**, 045014 (2010).
- J. Čapek, M. Hála, O. Zabeida, J. E. Klemberg-Sapieha, and L. Martinu, *J. Phys. D: Appl. Phys.* **46**, 205205 (2013).
- N. Brenning, C. Huo, D. Lundin, M. A. Raadu, C. Vitelaru, G. D. Stancu, T. M. Minea, and U. Helmersson, *Plasma Sources Sci. Technol.* **21**, 025005 (2012).
- D. Lundin, T. Minea, and J.-T. Gudmundsson, *High Power Impulse Magnetron Sputtering Fundamentals, Technologies, Challenges and Applications* (Elsevier, Amsterdam, 2020).
- H. Hajihoseini, M. Čada, Z. Hubička, S. Ünalı, M. A. Raadu, N. Brenning, J.-T. Gudmundsson, and D. Lundin, *J. Vac. Sci. Technol. A* **38**, 033009 (2020).

- ²³N. Brenning, A. Butler, H. Hajihoseini, M. Rudolf, M. A. Raadu, J.-T. Gudmundsson, T. Minea, and D. Lundin, *J. Vac. Sci. Technol. A* **38**, 033008 (2020).
- ²⁴O. Antonin, V. Tiron, C. Costin, G. Popa, and T. Minea, *J. Phys. D: Appl. Phys.* **48**, 015202 (2015).
- ²⁵A. Butler, N. Brenning, M. A. Raadu, J.-T. Gudmundsson, T. Minea, and D. Lundin, *Plasma Sources Sci. Technol.* **27**, 105005 (2018).
- ²⁶V. Tiron, I.-L. Velicu, I. Mihaila, and G. Popa, *Surf. Coat. Technol.* **337**, 484 (2018).
- ²⁷V. Tiron, I.-L. Velicu, O. Vasilovici, and G. Popa, *J. Phys. D: Appl. Phys.* **48**, 495204 (2015).
- ²⁸T. Shimizu, M. Zanaška, R. P. Villoan, N. Brenning, U. Helmersson, and D. Lundin, *Plasma Sources Sci. Technol.* **30**, 045006 (2021).
- ²⁹G. D. Stancu, N. Brenning, C. Vitelaru, D. Lundin, and T. Minea, *Plasma Sources Sci. Technol.* **24**, 045011 (2015).
- ³⁰S. Konstantinidis, J. P. Dauchot, M. Gangiu, A. Ricard, and M. Hecq, *J. Appl. Phys.* **99**, 013307 (2006).
- ³¹Z. Hubička, S. Kment, J. Olejníček, M. Čada, T. Kubart, M. Brunclíková, P. Kšírová, P. Adámek, and Z. Remeš, *Thin Solid Films* **549**, 184 (2013).
- ³²T. Kubart, M. Čada, D. Lundin, and Z. Hubička, *Surf. Coat. Technol.* **152**, 238 (2014).
- ³³K. M. Green, D. B. Hayden, D. R. Juliano, and D. N. Ruzic, *Rev. Sci. Instrum.* **68**, 12 (1997).
- ³⁴L. Meng, R. Raju, R. Flauta, H. Shin, D. N. Ruzic, and D. B. Hayden, *J. Vac. Sci. Technol. A* **28**, 112 (2010).
- ³⁵P. Poolcharuansin, M. Bowes, T. J. Petty, and J. W. Bradley, *J. Phys. D: Appl. Phys.* **45**, 322001 (2012).
- ³⁶N. Brenning, J.-T. Gudmundsson, M. A. Raadu, T. J. Petty, T. Minea, and D. Lundin, *Plasma Sources Sci. Technol.* **26**, 125003 (2017).
- ³⁷A. Revel, A. el Farsy, L. de Poucques, J. Robert, and T. Minea, *Plasma Sources Sci. Technol.* **30**, 125005 (2021).
- ³⁸D. Lundin, P. Larsson, E. Wallin, M. Lattemann, and N. Brenning, *U. Helmersson Plasma Sources Sci. Technol.* **17**, 035021 (2008).